An Optical Fiber Bragg Grating Sensing System for Scour Monitoring

Zhi Zhou^{1,2,3,*}, Minghua Huang², Liqing Huang², Jinping Ou^{1,2} and Genda Chen³

¹School of Civil Engineering, Dalian University of Technology, Dalian, 116024, China
 ²School of Civil Engineering, Harbin Institute of Technology, Harbin, 150090, China
 ³Center for Infrastructure Engineering Studies, Missouri University of Science and Technology, Rolla, MO 65409-0710, USA

Abstract: This paper proposes an optical fiber Bragg grating (FBG) sensing system for scour monitoring around the foundations of bridge piers and abutments. The new system introduces a uniform-strength fiber-reinforced polymer (FRP) beam that is instrumented with two FBG sensors in two sides of its neutral axis. The tensile and compressive strains of the beam are measured under a hydrodynamic pressure as water flowing around bridge foundations. By assuming equal temperatures around the uniform-strength beam, the difference in wavelength variations of the two embedded FBG sensors was found to be proportional to the square of flow velocity, which is directly related to scour. A prototype scour sensing system was designed and fabricated to test its sensing property in the laboratory. The experimental results indicate that the proposed system is sensitive to flow change and further monitor the scour process effectively, without responding to its surrounding hydrostatic and soil pressures.

Key words: scour monitoring, optical fiber Bragg grating sensor, uniform-strength beam, fiber-reinforced polymer, sensing property.

1. INTRODUCTION

Scouring process is a phenomenon that is developed as deposits are removed from around the foundations of hydraulic and ocean engineering structures such as bridges, dams, and offshore platforms. Caused by swiftly flowing water (Boorstin 1987), scour often leads to a drastic reduction in the safe capacity and structural stability or results in structure failures as demonstrated by many incidences around the world. In the United States alone, approximately 60% of over 1500 bridges collapses since 1950s were caused by foundation scouring (Harik et al. 1990; Wardhana and Hadipriono 2003; Lagasse et al. 2007; Liang et al. 2009). For example, the New York State Thruway Bridge over Schoharie Creek collapsed without warning on April 5, 1987, which took the lives of ten persons (Daniel and Anthony 1991). In the upper Mississippi and lower Missouri River basins, at least 22 bridges failed at an estimated cost of more than \$8M during the 1993 flood (Kamojjala *et al.* 1994; Peggy and Daniel 1998). Therefore it is important to monitor the scour process of the foundations for an early identification of potential structure failures.

In the past two decades, a number of scour monitoring methods have been developed, including Diving, Physical Probes, RC boat, Ground Penetration Radar (GPR), Float-Out Device, Sonar, Magnetic Sliding Collar (Forde *et al.* 1999; Lagasse *et al.* 2001; Fukui and Otuka 2002; Anderson *et al.* 2007; Okoshi and Fukui 2001). As of 2005, they have been applied in approximately 100 bridges (Hunt 2004, 2005). However, it is still a challenge to match the reliability and durability of monitoring technologies with the long service life of bridges due to that most of these techniques have limited applications (Chang *et al.* 2004). Scour depth monitoring systems require reliable and robust real-time sensors that can be easily installed and that can sustain harsh condition of flooding.

^{*}Corresponding author. Email address: zhouzhi@dlut.edu.cn; Fax & Tel: +86-411-8470-9716.

A scour monitoring device based on an optical fiber Bragg grating (FBG) sensor offers a possible solution as tested by Lin *et al.* (2004, 2006). However, the sensor's readings are significantly influenced by hydrostatic and soil pressures, both of which increase with foundation depth. This paper proposes a new scour sensing system by introducing two FBG sensors to cancel out the effects of hydrostatic and soil pressures. The sensitivities of the new system to those effects and the variations in water flow velocity are investigated with a prototype measurement system. The underlying measurement principle of the proposed system is analytically studied and validated by laboratory tests.

2. THE PROPOSED SENSING SYSTEM AND ITS INSTALLATION

The concept of structural behavior monitoring has recently been introduced to assess various structural behaviors (Chen 2009). One of its main characteristics is to transfer the change in structural behavior into a sensing system so that the measured data is directly related to the structural behavior e.g. scour. Scour around a bridge pier locally alters the velocity of water flow, inducing a significant change in hydrodynamic pressure on the pier. The sensing system designed in this study is based on the differential pressure caused by flow.

Figure 1 illustrates the configuration of a bridge scour monitoring system that can be installed along a bridge pier, which mainly consists of a protective steel anchor, distributed sensing modules, transmission fibers and data acquisition system. As depicted in Figure 2, the

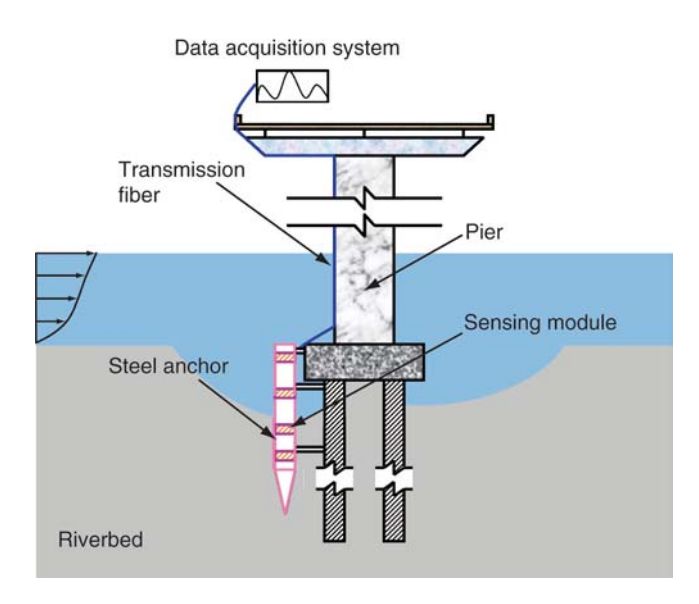


Figure 1. The proposed scour monitoring system and installation

distributed sensing modules are installed on the protective steel anchor and they mainly consist of two membrane sheets, one uniform-strength beam instrumented with two FBG sensors in two sides of its neutral axis, one transverse rod and one drum-like shell for fixing and supporting the membrane sheets and the uniform-strength beam. The transverse rods were fixed at the centers of the membrane sheets and connected to the free end of the uniform-strength beam. When the two membrane sheets deform subjected to pressure difference, the transverse rod will move and further result in the uniform-strength beam deform obviously and the embedded FBG sensors'

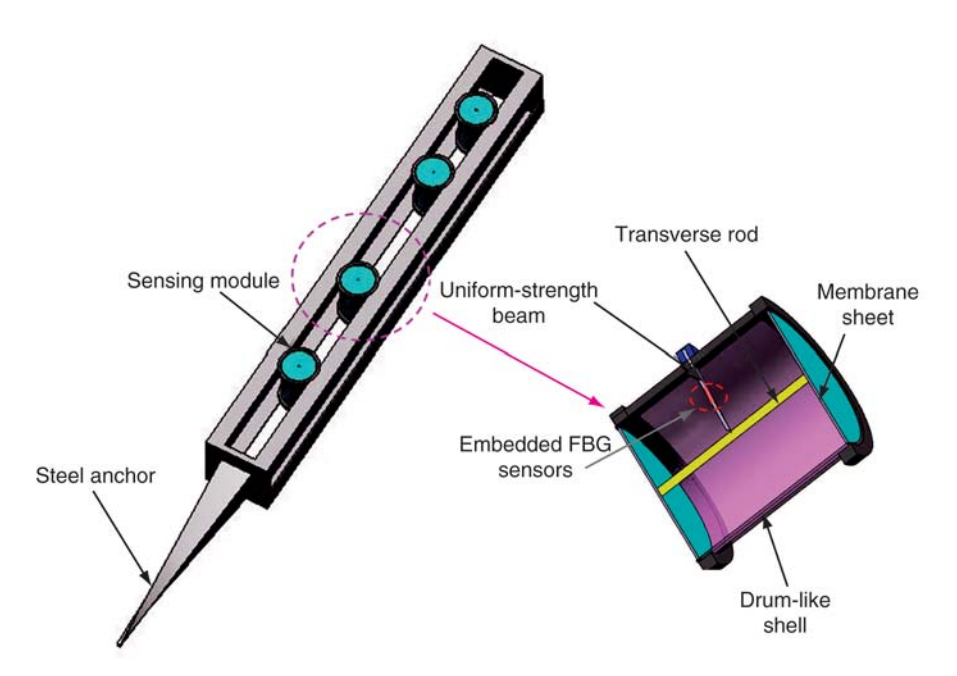


Figure 2. Sensing module's structure and installation

readings will change notably. Therefore this proposed system can monitor scour process accompanied with hydrodynamic pressures' differences.

In the practice, the protective steel anchor can be either hammered into the riverbed or fixed on the wall of a pier to keep the membrane sheets perpendicular to flow direction, then the membrane sheets bear larger pressure difference and the uniform-strength arise more notable strain resulted from the flow changes after the scour occurs around the pier, and further the FBG sensors monitor the scour process effectively.

3. UNDERLYING MEASUREMENT PRINCIPLE OF THE SENSING SYSTEM

Before scouring, the sensing module is set up in static water or buried in a riverbed, the two membrane sheets are subjected to equal hydrostatic and soil pressures as illustrated in Figure 3(a). In this case, the uniformstrength beam will not deform notably according to the equilibrium of forces, and the embedded FBG sensors' signal will virtually remain unchanged. However, as the river deposits erode away, the sensing module is exposed to water flow around a vertical pier, whose front bears the positive hydrodynamic pressure (punching pressure) while back suffers negative hydrodynamic pressure (suction pressure). Therefore membrane sheets would suffer unequal hydrodynamic pressure as shown in Figure 3(b). Subjected to the unequal hydrodynamic pressure, the two membrane sheets of the sensing module would deform obviously and result in the transverse rod which was fixed at the two membrane sheets start moving, then the uniform-strength beam arise notable strains and the embedded FBG sensors' readings change notably.

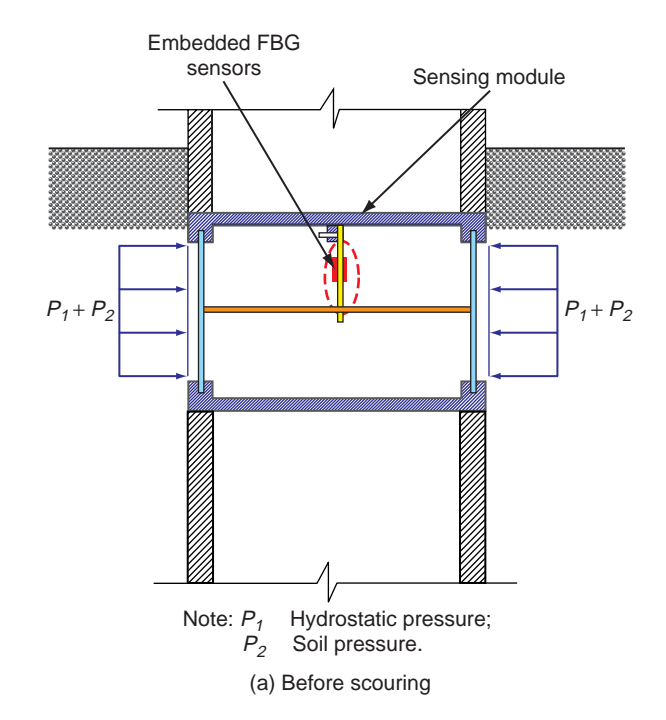
The unbalanced hydrodynamic pressure acting on the membrane sheets arises from the drag force, F_D , which is given by (Lin *et al.* 2006; Spurk and Aksel 2008):

$$F_D = C_D \frac{\rho v^2}{2} A_m \tag{1}$$

where, C_D is drag coefficient, A_m is the area of the membrane sheet, ρ is the water density, and ν is the flow velocity.

As shown in Figure 4, considering deformation compatibility condition between the central displacements of the membrane sheets and the displacement at the free end of the uniform-strength beam resulted from the rigid connecting effect of the transverse rod, these displacements δ can be calculated from the following equation:

$$\delta = \frac{F_D}{W_{aa}} \tag{2}$$



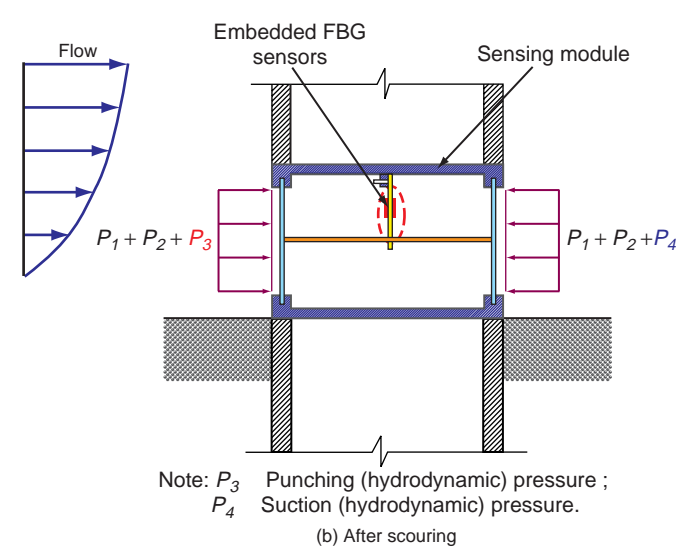
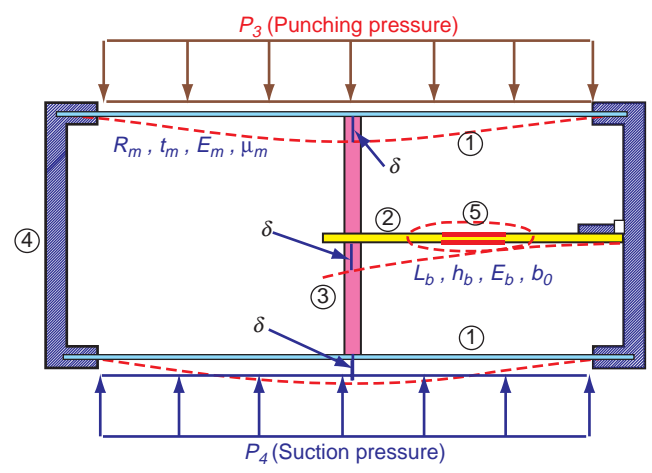


Figure 3. Loadings acting on the sensing module

in which W_{eq} is the equivalent flexural stiffness of the two membrane sheets and the uniform-strength beam and given by (Timoshenko and Krieger 1959; Liang *et al.* 2001):

$$W_{eq} = \frac{32\pi E_m t_m^3}{3(1 - \mu_m^2)R_m^2} + \frac{E_b b_0 h_b^3}{6L_b^3}$$
 (3)

where, E_m and μ_m are the Young's modulus and the Poisson's ratio, and R_m and t_m are the radius and thickness of the membrane sheets; and E_b is the Young's modulus, and L_b , b_0 and h_b are the effective length,



Note: $P_3 + P_4 = F_D / A_m$

- Membrane sheets;
- 4)- Drum-like shell (rigid);
- 2 Uniform-strength beam;
- (5)- Embedded FBG sensors. 3 - Transverse rod (rigid);

Figure 4. Deformation and loading state of the sensing module

width at the fixed end and height of the uniform-strength beam, respectively. Then for the uniform-strength beam, the strains ε_i at the location of the i th (i = 1, 2) embedded FBG sensor can be obtained following the relationship between the strains and the displacements at the free end (Liang et al. 2001):

$$\varepsilon_i = \frac{2y_i \delta}{L_h^2} \tag{4}$$

in which y_i is the distance of the embedde location of the i th (i = 1,2) FBG sensor from the neutral axis of the uniform-strength beam.

The wavelength change $(\Delta \lambda_{Bi})$ of the *i* th (i = 1,2)FBG sensor has been investigated as the effects of the applied strain (ε_i) and temperature difference (T_i) from the sensors' calibrations (Hill and Meltz 1997; Zhou 2003):

$$\Delta \lambda_{Ri} = K_{\varepsilon} \varepsilon_i + K_T T_i \quad (i = 1, 2) \tag{5}$$

where $\Delta \lambda_{Bi}$ is the variation of the central wavelength, and K_{ε} and K_{T} represent the strain and temperature sensing coefficients of of the FBG sensors, respectively. Assuming equal temperatures around the uniformstrength beam, that is $T_1 = T_2$, and apply these in Eqns 2 to 5, it yeilds:

$$\Delta \lambda_{R1} - \Delta \lambda_{R2} = \alpha V^2 \tag{6}$$

where, α is denoted as the sensing coefficient of the sensing module and expressed as:

$$\alpha = \frac{K_{\varepsilon}C_{D}\rho(y_{1} - y_{2})}{\left[\frac{32E_{m}t_{m}^{3}}{3(1 - \mu_{m}^{2})R_{m}^{4}} + \frac{E_{b}b_{0}h_{b}^{3}}{6\pi L_{b}^{3}R_{m}^{2}}\right]L_{b}^{2}}$$
(7)

4. DESIGN AND VALIDATION OF THE PROTOTYPE SENSING SYSTEM

4.1. Optimization of the Dimension Parameters

Eqn 7 indicates that the sensing coefficient α of the sensing module is influenced by the dimensions of the membrane sheets and the uniform-strength beam, which would be higher with the increases of the radius R_m of the membrane sheets, while lower with the increases of the thickness t_m of the membrane sheets, the height h_b and the width b_0 of the uniform-strength beam. With the increase of the effective length L_b of the uniformstrength beam, the sensing coefficient α initially increases and then decreases after reaching at its peak value; Similarly, Eqn 2 indicates that the displacement δ of the sensing module is also influenced by the dimensions of the membrane sheets and the uniformstrength beam, which increase with the increase of radius R_m of the membrane sheets and the effective length L_b of the uniform-strength beam, while decreases with the increases of the thickness t_m of the membrane sheets, the height h_b and the width b_0 of the uniform-strength beam. Therefore the dimensional parameters of the membrane sheets and uniform-strength beam should be optimized for the sensing module's design to provide a higher sensing coefficient under a reasonable displacement.

In the practices, the radius R_m of the membrane sheets and the effective length L_b of the uniform-strength beam, which are determined according to the maximum size of the sensing module, should be designed to match the requirements of the monitoring field and equal to each other for simplifying the design in general, so that only the influences of the thickness t_m of the membrane sheets, the height h_b and the width b_0 of the uniformstrength beam on the sensing coefficient α and the displacement δ were studied. Assuming that $R_m = L_b$, and let $t_m = \beta_1 R_m$, $h_b = \beta_2 L_b$ and $b_0 = \beta_3 L_b$, Eqns 2 and 7 can be seperately simplified as:

$$\delta = 3\pi C_D \rho \left(1 - \mu_m^2\right) R_m v^2 \cdot \psi \left(\beta_1, \beta_2, \beta_3\right) \tag{8}$$

$$\alpha = \frac{6\pi K_{\varepsilon} C_D \rho \left(1 - \mu_m^2\right) \left(y_1 - y_2\right)}{R_m} \cdot \psi \left(\beta_1, \beta_2, \beta_3\right) \tag{9}$$

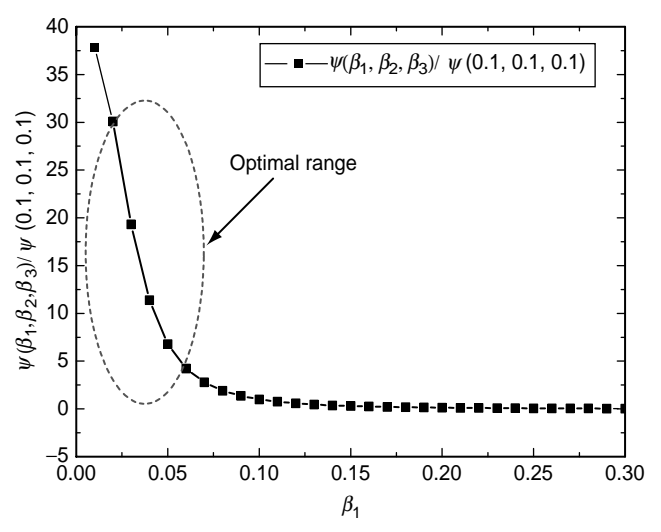
in which $\psi(\beta_1, \beta_2, \beta_3) = 1/[64\pi\beta_1^3 E_m + \beta_2^3 \beta_3 E_b(1 - \mu_m^2)]$ is defined as evaluating function to assess their influences on the sensing coefficient α and the displacement δ .

Considering the excellent anti-corrosion and waterproof performances besides its light weight, polyethylene material (PE) was adopted to develop the membrane sheets, and its Young's modulus E_m and the Poisson's ratio μ_m were separately given as 800 MPa and 0.4, according to Chang's work (2004); and the FRP material was applied to develop the uniform-strength beam and its Young's modulus E_b was 50 GPa (Zhang et al. 2005). With these material parameters, the values of the evaluating function $\psi(\beta_1, \beta_2, \beta_3)$ were calculated and the results are presented in Figure 5 comparing with $\psi(0.1,0.1,0.1)$.

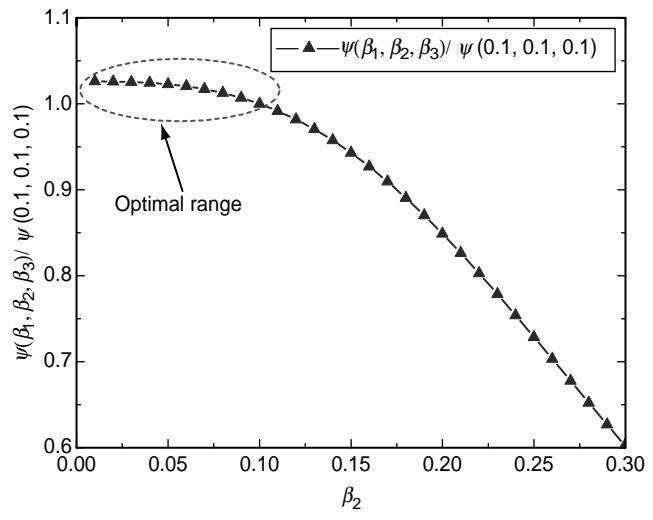
Figure 5 indicates that the thicknesses of membrane sheets are the dominant factors influencing the sensing coefficient and displacement of the sensing module, compared with the height and the width of the uniformstrength beam. Figure 5(a) presents that the sensing coefficient and the displacement decrease initially rapidly with the increase of the thickness of the membrane sheets, but increase slowly and approach the asymptotic value after the thickness reaching about 0.06 times of its radius. In order to provide a higher sensing coefficient, the membrane sheets of the sensing module should be thinner and thinner, but their flexural stiffness would be smaller and smaller. Once their flexural stiffness is too low, their central displacement would increase unstably and failed suddenly, when they are subjected to loading. To provide sufficient flexural stiffness and prevent these failures, the thicknesses of the membrane sheets are investigated as 1/100~1/5 times of their spans (Chen 2003). Therefore the thickness of the membrane sheets should be designed as 0.02~0.06 times of their radius, to provide higher sensing coefficient under a reasonable displacement. Figure 5(b) shows that the sensing coefficient and the displacement decrease initially slowly with the increase of the height of the uniform-strength beam while rapidly after the height reaching about 0.10 times of its effective length. Therefore the height of the uniform-strength beam should be less than 0.10 times of its effective length, to provide a high sensing coefficient under a reasonable displacement. Figure 5(c) indicates that the sensing coefficient and the displacement decrease linearly with the increase of the width of the uniform-strength beam, so that the uniform-strength beam should be narrower to provide a high sensing coefficient under a reasonable displacement.

4.2. Design of the Sensing Module

To test and verify the sensing property of the proposed sensing system, a sensing module has been designed and manufactured to establish the prototype sensing system



(a) The thickness of the membrane sheets



(b) The height of the uniform-strength beam

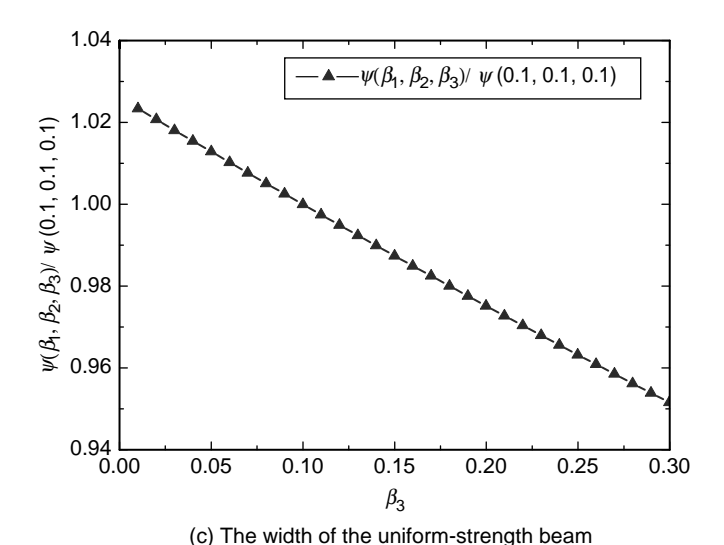


Figure 5. Dimension optimizations of the sensing module

in the laboratory. The sensing module was manufactured as follows: (1) preparing layers of glass fiber fabric, laying and fixing optical FBG sensors along the longitudinal direction between two adjacent layers, and then forming a FRP beam in the pultrusion machine, as shown in Figure 6(a); (2) shaping the FRP beam into an uniform-strength beam, as depicted in Figure 6(b); (3) connecting the middle of the transverse rod to the free end of the uniform-strength beam, fixing its two ends at the centers of the membrane sheets, and then fixing the uniform-strength beam and membrane sheets on the drum-like shell, as shown in Figure 6(c). Based on the above optimal results, the radius R_m and thickness t_m of the membrane sheets were designed as 50 mm and 1.2 mm; and the effective length L_b , height h_b and width b_0 of the uniform-strength beam were designed as 50 mm, 2.0 mm and 20 mm, respectively.

4.3. Location Calibration of the Embedded FBG Sensors

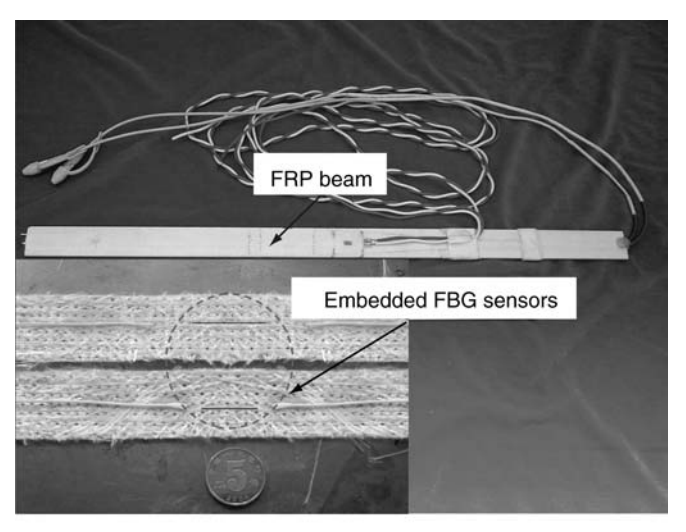
During the complicated pultrusion of the FRP beam, the previously designed embedded locations y_i of the FBG sensors might slightly change. In order to determine the sensing coefficient α of the sensing module accurately, it is necessary to calibrate the final embedded locations v_i of the FBG sensors. Before the FRP beam being shaped into an uniform-strength beam, a calibrating test was set up in the laboratory as shown in Figure 7. The length of the FRP beam was 600 mm, two electric resistance strain gauges (ES sensors) were attached to its surface on top and down of the embedded FBG sensors, and the FRP beam was applied a point load ranging from 0 N to 10 N at 2 N intervals for three loading loops. Under each loading step, the strains of the FRP beam were separately measured by ES sensors and given FBG sensors. The measured results are presented in Figure 8.

Figure 8 presents that the strains measured by two FBG sensors vary linearly with the increases of the applied loads and have good correlation with readings of the attached ES sensors; and the strain readings at three loading loop coincided with each other. Therefore the embedded FBG sensors can measure the strains of the FRP beam effectively.

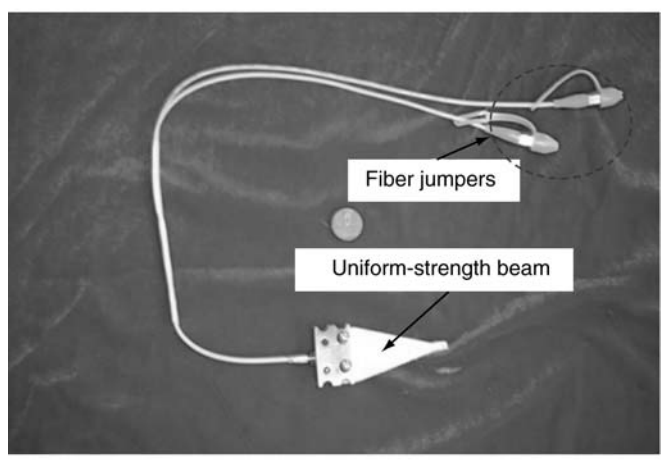
Basing on the measured strains, the embedded locations y_i of the FBG sensors can be calculated following:

$$y_i = \left(-1\right)^{i+1} \cdot \frac{\left(\varepsilon_i\right)_{FBG}}{\left(\varepsilon_i\right)_{FS}} \cdot \frac{h_b}{2} \tag{10}$$

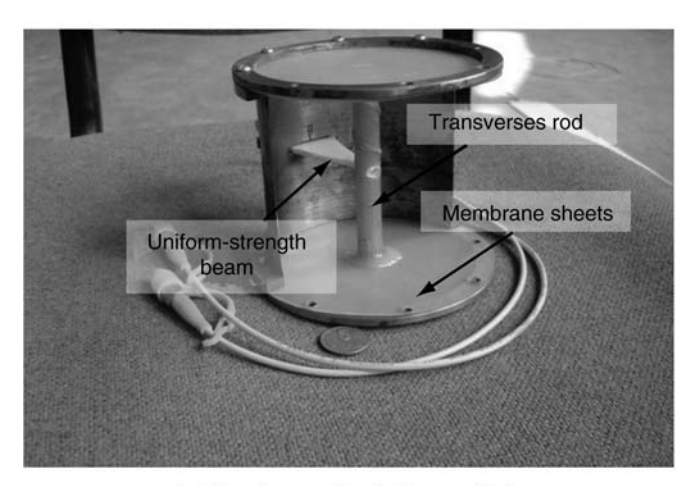
in which $(\varepsilon_i)_{FBG}$ and $(\varepsilon_i)_{ES}$ separately present the strain values measured by the *i* th embedded FBG sensors and



(a) FRP beam



(b) Uniform-strength beam



(c) Sensing module (before sealing)

Figure 6. Manufacture of prototype sensing module

attached ES sensors. The calculated results of each load steps are statistically presented in Figure 9, which provides that the embedded locations $(y_1 \text{ and } y_2)$ of the FBG sensors are separately 0.39mm and -0.70mm.

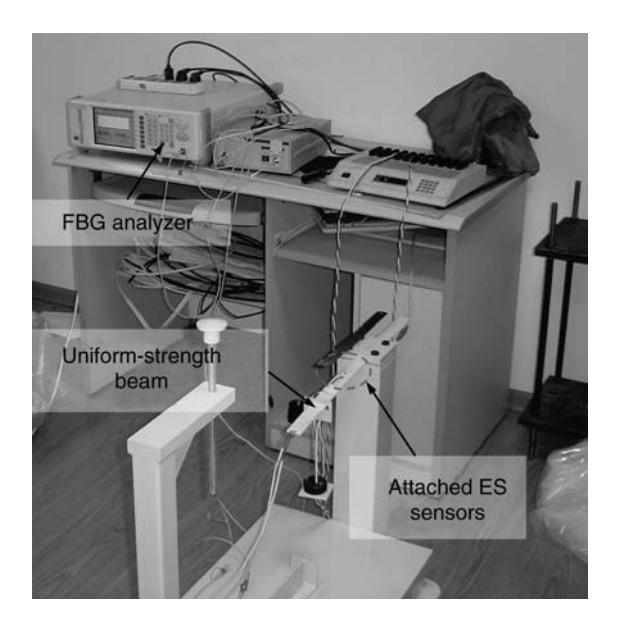
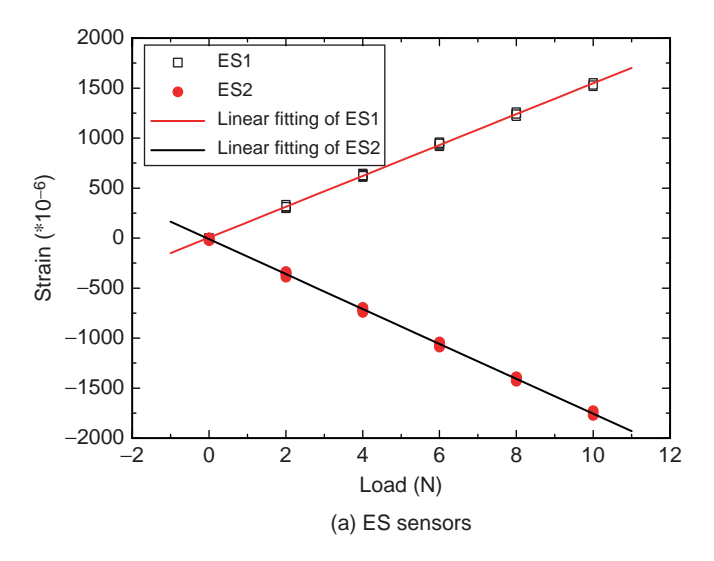


Figure 7. Test apparatus for calibrating FBG sensor's locations



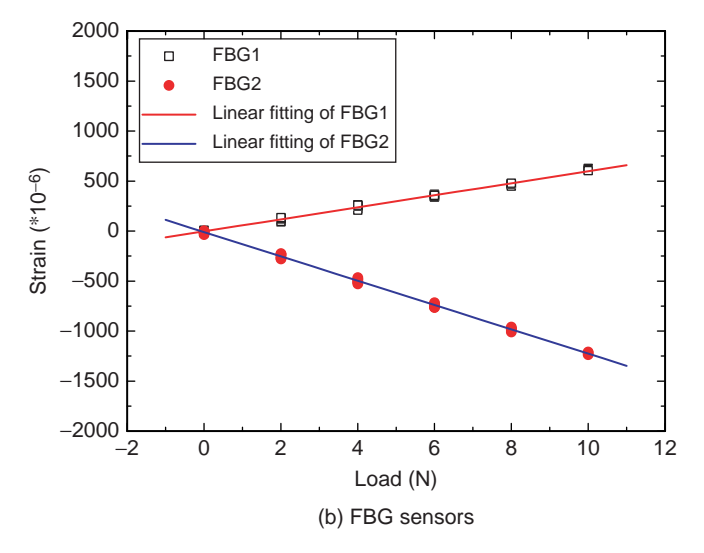
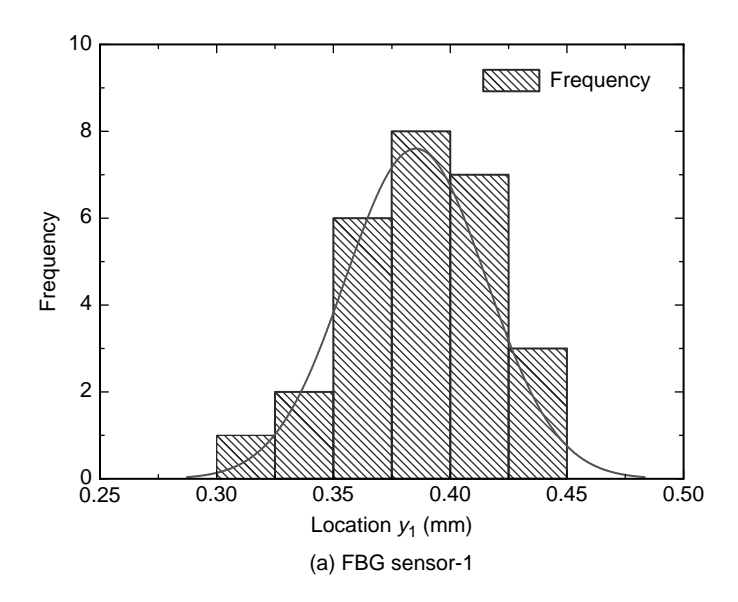


Figure 8. Strains measured results of FRP beam under a point load



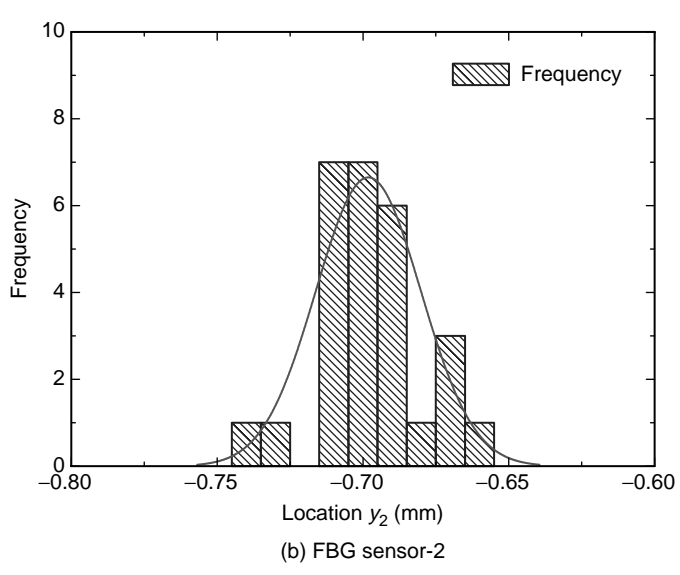


Figure 9. Locations of the embedded FBG sensors

4.4. Validation of the Prototype Monitoring System

With the designed sensing module, a prototype monitoring system was established in the laboratory to validate its sensing property. The calibrating test was set up as depicted in Figure 10: water starts flowing from the high end of the sink with a zero initial velocity and strikes the membrane sheets of the sensing module at the low end and the testing flow velocity (actual velocity) ranged from 0.6 m/s to 1.8 m/s, which were calculated following the law of energy conservation $v = \sqrt{2gh}$. Under each flow velocity, the central wavelengths of the embedded FBG sensors were recorded by the data acquisition system and their variations are presented in Figure 11.

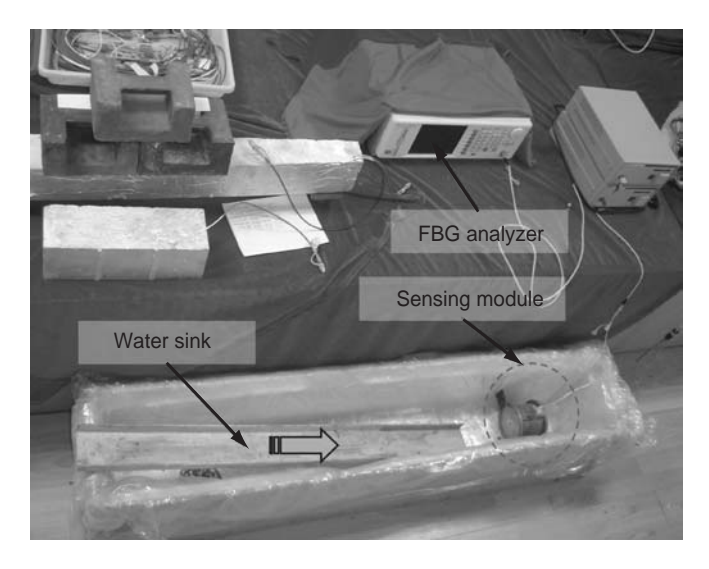


Figure 10. Calibration testing apparatus for proposed monitoring system

Figure 11 presents that the wavelength of FBG sensor 1 increases with the increases of the flow velocity while the wavelength of FBG sensor 2 decreases with the increases of the flow velocity, which means that FBG sensor 1 sensed the tensile strain while FBG sensor 2 sensed compressive strains. The wavelength variations measured at increasing and decreasing processes of the flow velocity agreed well with each other.

Resulted from the low adhesion force of water flow, the Reynolds Number in the testing was larger than 10^3 under the testing flow velocity, so that the drag coefficient C_D can be given as 1.17 (Kreith *et al.* 1999). Let the strain sensing coefficient K_{ε} of the FBG sensors were $1.2 \,\mathrm{pm}/\mu\varepsilon$ (Zhou 2003), the theoretical value of the sensing coefficient α calculated as $146.0 \,\mathrm{pm \cdot s^2/m^2}$ following Eqn 7. Further, according to the measured wavelength variations of the embedded FBG sensors, the flow velocities (measured velocities) were obtained following Eqn 6. The results are presented in Figure 12, compared with the actual velocities.

Figure 12 presents that the measured velocities agree well with the actual velocities and the measured values were less than the actual velocities. With the increase of the flow velocities, the measured errors increased slightly and the maximum error was about +0.10 m/s.

Figure 13 shows the relationship between the difference of the wavelength variations and the square of the flow velocities. Its linear fitting has a correlation coefficient of 0.9982 and provides a sensing coefficient α of 129.6 pm · s²/m², which is coincided with the theoretical value 146.0 pm · s²/m². Therefore the prototype monitoring system can measure the flow change and further monitor the scour process effectively.

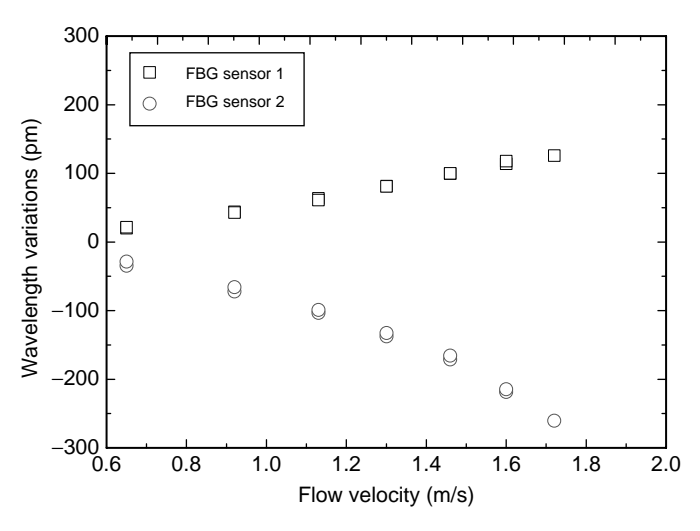
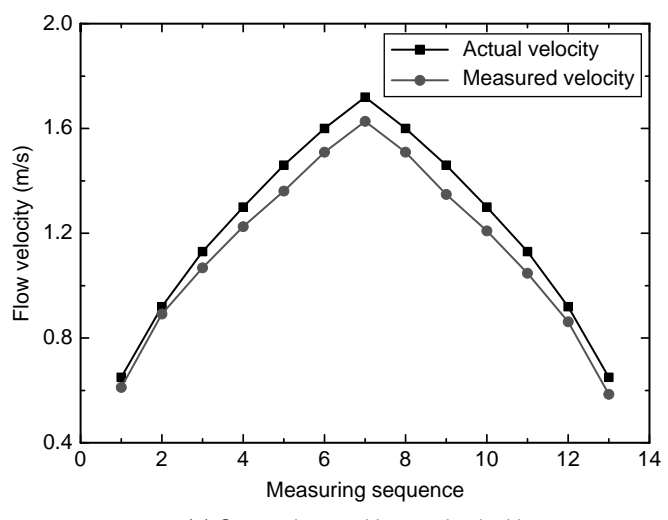


Figure 11. Relationship between wavelength variations and flow velocities



(a) Comparisons with actual velocities

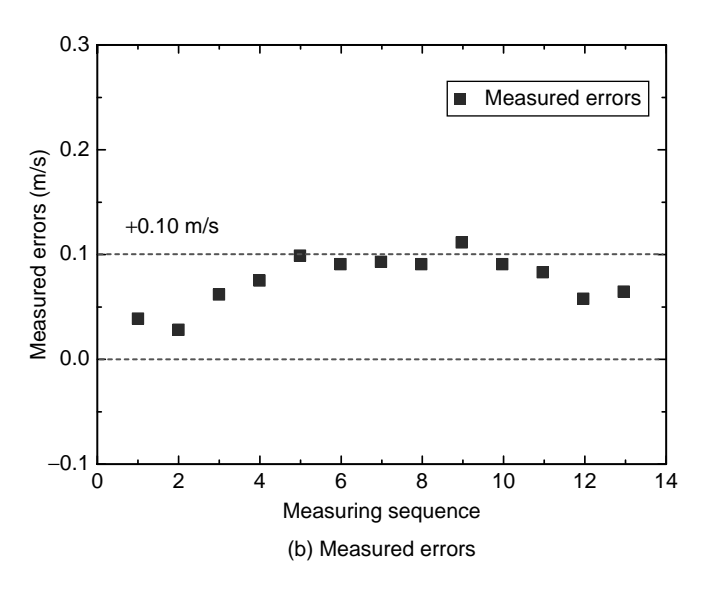


Figure 12. Measured results of the flow velocities

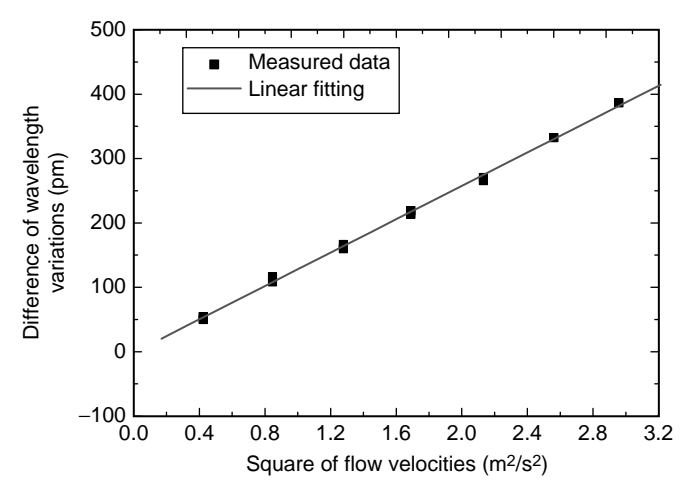
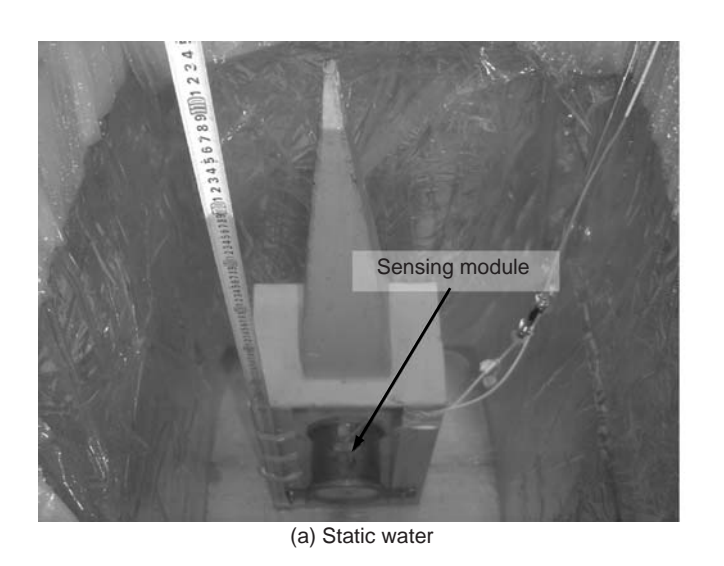


Figure 13. Relationship between the differences of wavelength variations and the square of flow velocities

4.5. Influences of Hydrostatic and Soil Pressures

To test the influences of hydrostatic and soil pressures on the sensing property of the proposed monitoring system, a sensing module was submerged into static water and soil deposits in sequence and the testing setups are depicted in Figure 14. In the test, the depth of static water varied from 0.1 m to 1.0 m and the depth of soil deposits varied from 0 m to 0.4 m. The central wavelengths of the embedded FBG sensors 1 and 2 were recorded, and their wavelength variations and differences were calculated, which are separately presented in Figures 15 and 16.

Figure 15 indicates that the central wavelengths of the embedded FBG sensors 1 and 2 fluctuated with the increases of the water and the soil deposits' depth and



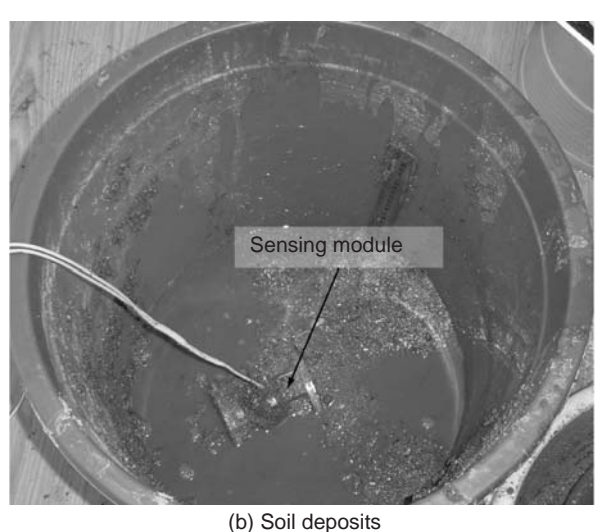
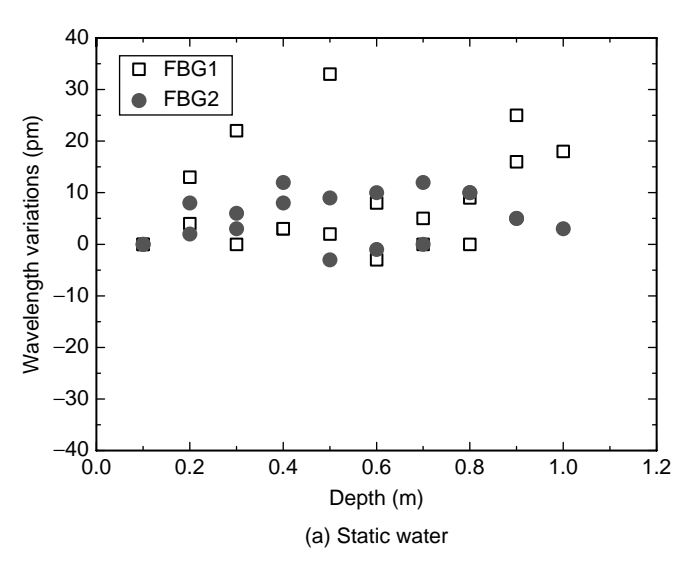


Figure 14. Apparatus for testing the influences of the depths' change



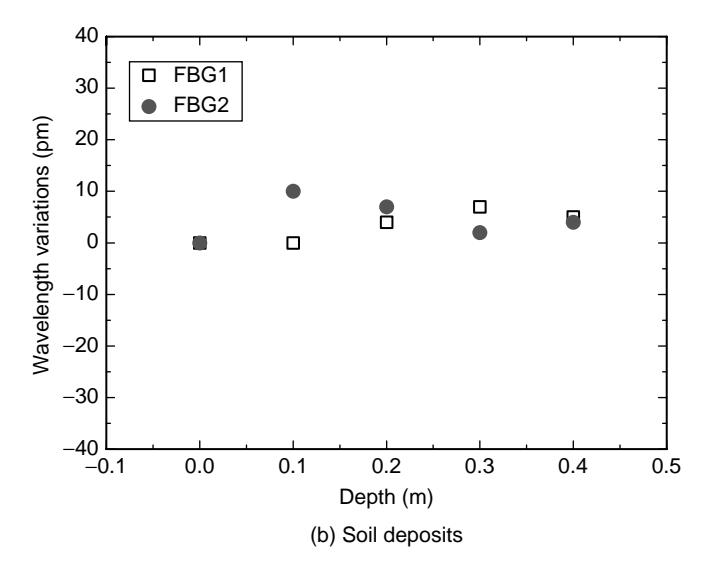


Figure 15. Relationship between wavelength variations and the depths

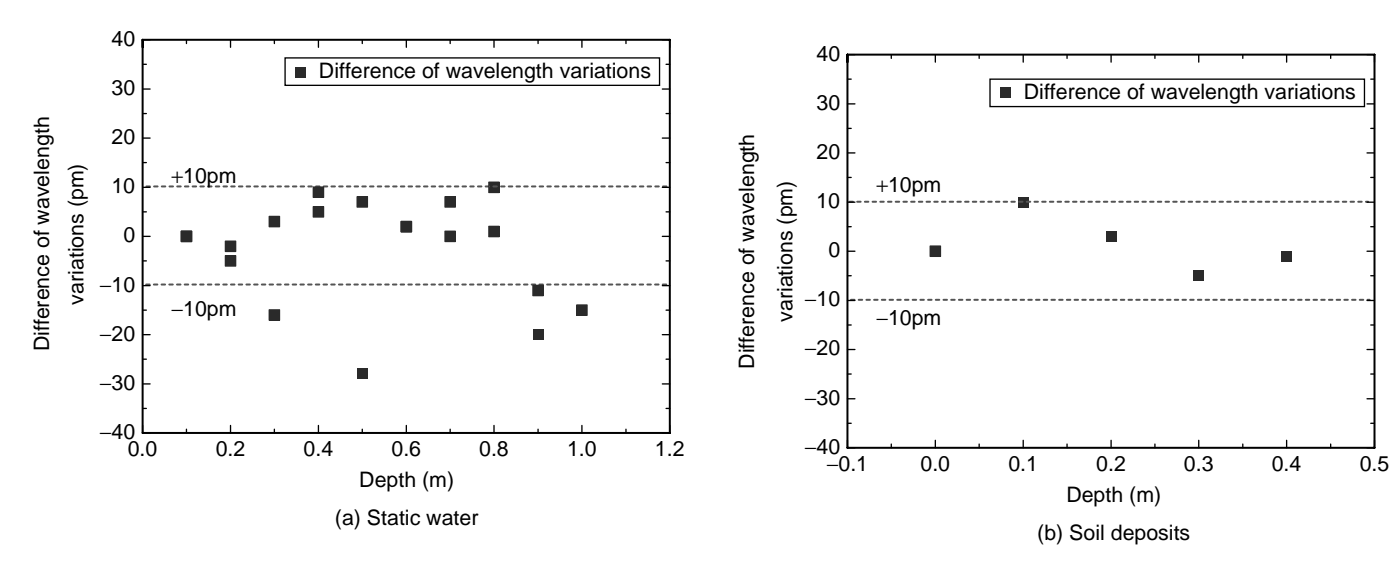


Figure 16. Relationship between differences of wavelength variations and the depths of (a) static water, and (b) soil deposits

the maximum fluctuations were separately about 25 pm and 10 pm. Figure 16 presents that the differences between the wavelength variations of the FBG sensors 1 and 2 fluctuated around zeros and mostly bounded in −10 pm ~+10 pm. Coleman and Melville (2001) studied the bridge scour experiences in New Zealand and presented that the critical velocity of the bridge's local scour was generally about 3 m/s. In this flow environment, it can be founded that 0.02 m/s flow changes would result in more than 15 pm wavelength variations' difference according to the calibration sensing coefficient, which is larger than that resulted from the depth variations of static water and soil deposits. Therefore the influences of static water and soil deposit are slight and can be neglected in the scour monitoring practices, especially in the monitoring applications of the bridge local scours.

5. CONCLUSIONS

To improve the durability and reliability of conventional scour monitoring sensors based on electrical gauges, a novel type of optical FBG monitoring systems has been developed. Based on the discussions of its underlying principle, the analysis of the dimension parameters and the laboratory tests with a prototype sensing system, the following conclusions can be drawn:

- a) The sensing modules installed in the proposed scour monitoring system are directly related to the hydrodynamic pressure distribution of water flow around a bridge pier, a root cause for bridge scour, so that scour depth can be monitored and determined reliably;
- b) The thickness of the membrane sheets is the dominate factor of the sensing property of the sensing module and should be designed as

- 0.02~0.06 times of its radius, and the height of the uniform-strength beam should be less than 0.10 times of its effective length;
- c) The proposed monitoring system can measure the flow change and further monitor the scour process effectively, and the influences of hydrostatic and soil pressures are slight and can be neglected in the scour monitoring practices, especially in the bridge local scours monitoring.

ACKNOWLEDGEMENTS

The authors are grateful for the financial support from National Natural Science Foundation of China (NSFC) under Grants. 10672048 and 50978079, and also thank the two careful anonymous reviewers for their comments and kind suggestions.

REFERENCES

Anderson, N.L., Ismael, A.M. and Thitimakorn, T. (2007). "Ground-penetrating radar: a tool for monitoring bridge scour", *Environmental & Engineering Geosciences*, Vol. 13, No. 1, pp. 1–10.

Boorstin, R.O. (1987). "Bridge collapses on the thruway: trapping vehicles", *The New York Times*, Vol.CXXXVI, No. 47, pp. 101–108.

Chang, H.Z. (2004). *Mechanics of Materials*, 2nd Edition, Higher Education Press, Beijing, China. (in Chinese)

Chang, W.Y., Lai, J.S. and Yen, C.L. (2004). "Evolution of scour depth at circular bridge piers", *Journal of Hydraulic Engineering*, ASCE, Vol. 130, No. 9, pp. 905–913.

Chen, G.D. (2009). "Why do we need structural behavior monitoring", *Proceedings of Annual ANCRISST Conference*, Northeastern University, Boston, USA, July.

Chen, J. (2003). *Stability of Steel Structures-Theory and Design*, 2nd Edition, Science Press, Beijing, China. (in Chinese)

- Coleman, S.E. and Melville, B.W. (2001). "Case study: New Zealand bridge scour experiences", *Journal of Hydraulic Engineering*, ASCE, Vol. 127, No. 7, pp. 535–546.
- Daniel, V.S. and Anthony, R.I. (1991). "The collapse of the Schoharie Creel Bridge: a case study in concrete fracture mechanics", *International Journal of Fracture*, Vol. 51, No. 1, pp. 73–92.
- Forde, M.C., McCann, D.M., Clark, M.R., Broughton, K.J., Fenning, P.J. and Brown, A. (1999). "Radar measurement of bridge scour", NDT&E International, Vo. 32, No. 8, pp. 481–492.
- Fukui, J. and Otuka, M. (2002). "Development of the new inspection method on scour condition around existing bridge foundations", First International Conference on Scour of Foundation, University Drive East, College Station, Texas, USA.
- Harik, E.I., Shaaban, A.M., Gesund, H., Valli, G.Y.S. and Wang, S.T. (1990). "United States bridge failures, 1951-1988", *Journal of Performance of Constructed Facilities*, ASCE, Vol. 4, No. 4, pp. 272–277.
- Hill, K.O. and Meltz, G. (1997). "Fiber Bragg grating technology fundamentals and overview", *Journal of Lightwave Technology*, Vol. 15, No. 8, pp. 1263–1276.
- Hunt, B.E. (2005). "Establishing a scour monitoring", *GSP 135 Erosion of Soil and Scour of Foundations*, pp. 1–11.
- Hunt, B.E. (2005). Practices for Monitoring Scour Critical Bridges, First Draft Report for NCHRP Project 20-5, U.S. Transportation Research Board.
- Lagasse, P.F., Clopper, P.E., Zevenbergen, L.W. and Girard, L.W. (2007). Countermeasures to Protect Bridge Pier from Scour, NCHRP Report-593, Transportation Research Board, Washington DC.
- Lagasse, P.F., Zevenbergen, L.W., Schall, J.D. and Clopper, P.E. (2001). *Bridge Scour and Stream Instability Countermeasures: Experience, Selection, and Design Guidance*, 2nd Edition, Technical Report of U.S. Department of Transportation, Washington D.C., USA.
- Liang, F.Y., Benntt, C.R., Parsons, R.L., Han, J. and Lin, C. (2009).
 "A literature review on behavior of scoured piles under bridges",
 International Foundation Congress & Equipment Expo 2009-In
 Site Testing, Analysis, and Reliability of Foundations,
 pp. 482–489.
- Liang, L.B., Zhang, W.G., Zhao, Q.D., Liu, Z.G., Dong, X.Y., Ye, J.T., Yang, C.N. and Hu, D.J. (2001). "Analyses and measurement of strain based on fiber Bragg grating sensors", *Journal of Optoelectronics-Laser*, Vol. 12, No. 11, pp. 1152–1155. (in Chinese)
- Lin, Y.B., Chern, J.C., Chang, K.C., Chang, Y.W. and Wang, L.A. (2004). "The utilization of fiber Bragg grating sensors to monitor high performance concrete at elevated temperature", *Smart Material and Structures*, Vol. 13, No. 4, pp. 784–790.
- Lin, Y.B., Lai, J.S., Chang, K.C. and Li, L.S. (2006) "Flood scour monitoring system using fiber Bragg grating sensors", Smart Materials and Structures, Vol. 15, No. 6, pp. 1950–1959.

- Kamojjala, S., Gattu, N.P., Parola, A.C. and Hagerty, D.J. (1994). "Analysis of 1993 upper Mississippi flood highway infrastructure damage", *Proceeding of the First International Conference on Water Resource Engineering*, pp. 1061–1065.
- Kreith, F., Berger, S.A. et al. (1999). *Fluid Mechanics*, Boca Raton: CRC Press LLC.
- Okoshi, M. and Fukui, J. (2001) "Present state of investigation technique for scouring", *The Foundation Engineering and Equipment*, Vol. 29, No. 9, pp. 19–21.
- Peggy, A.J. and Daniel, A.D. (1998). "Probabilistic bridge scour estimate", *Journal of Hydraulic Engineering*, ASCE, Vol. 124, No. 7, pp. 750–754.
- Spurk, J.H. and Aksel, N. (2008). *Fluid Mechanics*, 2nd Edition, Springer, Berlin Heidelberg, Germany.
- Timoshenko, S.P. and Krieger, S.W. (1959). *Theory of Plates and Shells*, 2nd Edition, McGraw-Hill Book Company, Inc.
- Wardhana, K. and Hadipriono, F.C. (2003). "Analysis of recent bridge failures in the united states", *Journal of Performance of Constructed Facilities*, Vol. 17, No. 3, pp. 144–150.
- Zhang, X.Y., Ou, J.P., Wang, B. and He, Z. (2005). "Comparison experimental study on mechanical property of different GFRP bars", *FRP/CM*, Vol. 32, No. 2, pp. 9. (in Chinese)
- Zhou, Z. (2003). Optical Fiber Smart Bragg Grating Sensors and Intelligent Monitoring Systems of Civil Infrastructures, PhD Thesis, The Harbin Institute of Technology, Harbin, China. (in Chinese)

aman of the manhuman cheets

NOTATION

A_m	area of the membrane sheets		
b_0	width at the fixed end of the uniform-		
	strength beam		
C_D	drag coefficient		
E_b	Young's modulus of the uniform-		
U	strength beam		
E_m	Young's modulus of the membrane		
m	sheets		
F_D	drag force		
h_b	height of the uniform-strength beam		
L_b	effective length of the uniform-strength		
	beam		
$K_{arepsilon}$	strain sensing coefficient of FBG sensor		
K_T	temperature sensing coefficient of FBG		
	sensor		
R_m	radiu of the membrane sheets		
T_i	temperature difference		
t_m	thickness of the membrane sheets		
W_{eq}	equivalent flexural stiffness of the		
1	sensing module		
y_i	location of the i th ($i = 1,2$) FBG sensor		
	distance from the neutral axis		
α	sensing coefficient of the sensing		
	module		
β_1 , β_2 and β_3	proportions of t_m/R_m , h_b/L_b and b_0/L_b		

$\Delta \lambda_{Bi}$	wavelength change of the i th $(i = 1,2)$	$\psi(\beta_1,\beta_2,\beta_3)$	evaluating function to assess the
	FBG sensor		influences of the dimensions
δ	displacement	ρ	water density
\mathcal{E}_i	strain at the location of the i th ($i = 1,2$)	μ_m	Poisson's ratio of the membrane sheets
	FBG sensor	ν	flow velocity

Copyright of Advances in Structural Engineering is the property of Multi-Science Publishing Co Ltd and its content may not be copied or emailed to multiple sites or posted to a listserv without the copyright holder's express written permission. However, users may print, download, or email articles for individual use.